ES Materials & Manufacturing

RESEARCH PAPER View Article Online

Simulation for the Influence of Interface Thickness on the Dendritic Growth of Nickel-Copper Alloy by a Phase-Field Method

Yuhong Zhao,[1*] Bing Zhang,[1] Weipeng Chen,[1] Hong Wang,[1] Meng Wang[2] and Hua Hou[1*]

Based on the WBM II (Wheeler-Boettinger-McFadden) phase-field model, the solute concentration at the solid-liquid interface region was defined and analyzed to make it more consistent with actual solidification conditions. The interface thickness in the model was modified, and on this basis, the dendritic morphology and solute distribution during the growth of Ni-Cu alloy dendrite were simulated. The results show that with the interface thickness decreases, the secondary dendrite arms become more developed and the dendrite trunks become finer. The smaller the interface thickness, the thinner the solute diffusion layer at the solid-liquid interface frontier, and the solute at the frontier more easily diffuses into the adjacent liquid phase, thus the dendrite tip grows faster.

Keywords: Ni-Cu alloy; Phase-field method; Interface thickness; Solute field

Received 9 August 2018, **Accepted** 18 October 2018

DOI: 10.30919/esmm5f135

1. Introduction

Ni-Cu alloys are typical binary single-phase alloys, which have excellent properties and have a very wide range of applications in the industrial field. The interfacial morphology of solidified microstructure of Ni-Cu alloy not only relates to mechanical properties, but also is an important factor affecting corrosion resistance.[1,2]

The phase field method coupled with the external field has become a powerful tool for simulating the complex dendritic morphology during solidification because it does not require tracking of complex solid-liquid interface.[3,4] In 1992, Wheeler, Boettinger and McFadden[5] proposed the phase-field model of binary alloy isothermal solidification at the sharp interface limit (WBM I model), and used this model to simulate the dendritic morphology of Ni-Cu alloy. Subsequently, Wheeler *et al*.[6-8] proposed an improved alloy phase field model (WBM II model) containing the solute gradient correction term and obtained solute segregation calculation results consistent with experiments. In 1998, Kim *et al*.[9] derived a new alloy phase field model (KKS model) based on the assumption that the solid-liquid interface is a mixture of solid and liquid phases with the same chemical potential. Karma *et al*.[10,11] performed asymptotic analysis of the phase field model under the constraint of thin interface thickness, and obtained an effective Gibbs-Thomson relationship at a certain interface thickness, suggesting that the interface thickness can be larger than the capillary length. A phase-field model that can simulate large undercooling ranges was established. Loginova et al.[12] took into account the release of latent heat of crystallization, using an alternating direction implicit method (ADI algorithm) to simulate the non-isothermal solidification dendritic growth of Ni-Cu alloy; Provatas *et al*.[13] used adaptive mesh to simulate dendrite growth in two and three dimensions, which significantly improved the scale and computational efficiency of microstructure. Wu *et al*.[14] used phase-field method to study the solidification dendrite growth of Ni-Cu alloys under isothermal, non-isothermal and certain temperature gradients. Du *et al*.[15] studied the evolution of dendrite morphology of Ni-Cu alloys under forced convection using phase-field method coupled with the flow field. The results show that the increase of the flow rate will enhance the asymmetry of the dendritic morphology, leading to the transformation of dendrite to semi-circular morphology. Hou Chaojie *et al*.[16] studied the effect of undercooling on the dendritic morphology and microsegregation of Ni-Cu alloys using phase-field model coupled with thermal disturbances. Zhao Yuhong *et al*.[17] studied the influence of temperature field coupling strength on the growth of pure Ni dendrite using phase-field model of coupled temperature field. Wang Hong *et al*.[18] studied the 3D orientation transitions of dendrites under different anisotropic parameters.

In this paper, based on the free energy density function of the WBM II model, it is coupled with the concentration field equation and the temperature field equation, and an improved binary alloy phase field is constructed by analyzing the value and distribution of the interface thickness.

2. Phase field model

2.1 Phase Field Equations Coupled with Temperature Fields

In the WBM II model, the free energy density function containing $(\nabla c)^2$ term and $(\nabla \phi)^2$ term can be expressed as:[19]

$$F = \int_V \left[f(\phi,c,e) - \frac{1}{2}\varepsilon^2(\nabla\phi)^2 + \frac{1}{2}\delta^2(\nabla c)^2 \right] dV \quad (1)$$

[1]*School of Materials Science and Engineering, North University of China, Taiyuan 030051, China*
[2]*State Key Laboratory of Solidification Processing, Northwestern Polytechnical University, Xi'an 710072, China*
***E-mail:** zhaoyuhong@nuc.edu.cn; houhua@nuc.edu.cn*

where ε is the phase-field gradient coefficient, δ is the concentration field gradient coefficient, e is the internal energy term related only to the system temperature.

For pure substance A, its free energy density is expressed as:

$$f^A = TG^A(\phi) + e_s^A(T_m^A) - C^A T_m^A + p(\phi)L^A(1-\frac{T}{T_m^A}) - C^A T ln\frac{T}{T_m^A} \quad (2)$$

where C^A is the specific heat, L^A is the latent heat; e_s^A is internal energy density of substance A in solid phase; T_m^A is the melting point of substance A; $p(\phi) = \phi^3(10-15\phi+6\phi^2)$ is the potential function. $G^A(\phi) = W^A g(\phi)$, where $g(\phi) = \phi^2(1-\phi)^2$ is defined as a double-well function; There is the same free energy expression for substance B.

For ideal solutions, the chemical potentials are expressed as:

$$\mu_A^L = f^A(\phi,T) + \frac{RT}{V_m} ln\,(1+C_L) \quad (3)$$

$$\mu_B^L = f^B(\phi,T) + \frac{RT}{V_m} ln\,C_L \quad (4)$$

The approximate formula for melting free energy is:

$$\left[\mu_A^L - \frac{RT}{V_m}\ln(1-C_L)\right] - \left[\mu_A^S - \frac{RT}{V_m}\ln(1-C_S)\right] = \Delta H_{mA}(1-T/T_A) \quad (5)$$

$$\left(\mu_B^L - \frac{RT}{V_m} ln\,C_L\right) - \left[\mu_B^S - \frac{RT}{V_m} ln\gamma_B^S C_S\right] = \Delta H_{mB}(1-T/T_B) \quad (6)$$

where μ_A^S, μ_A^L, μ_B^S and μ_B^L is the chemical potentials of component A and B in solid and liquid, respectively. C_S, C_L is the solute concentration in solid and liquid, respectively. ΔH_{mA}, ΔH_{mB} is the melting heat of pure A and B, respectively. T_A, T_B is the melting point of A and B, respectively.

Substituting Eqs. (5) and (6) into (3) and (4) yields a relationship between μ_A^S and μ_B^L.

The solid-liquid interface is a mixture of solid and liquid phases with the different chemical concentration. When the system is in equilibrium, solid and liquid phases have the same chemical potential, so the free energy expression at the interface region can be expressed as:

$$f^A(\emptyset,c,T) = p(\emptyset)(1-C_L)\mu_A^L + [1-p(\emptyset)](1-C_S)\mu_A^S \quad (7)$$

$$f^B(\emptyset,c,T) = p(\emptyset)C_L\mu_B^L + [1-p(\emptyset)]C_S\mu_B^S \quad (8)$$

The total free energy of the solution can be expressed as:

$$f = p(\emptyset)\left[(1-C_L)\mu_A^L + C_L\mu_B^L\right] + [1-p(\emptyset)](1-C_S)\mu_A^S + C_S\mu_B^S] \quad (9)$$

Substituting Eqs. (3), (4), (7) and (8) into (9), the phase-field evolution equation obtained by derivation can be expressed as:

$$\frac{\partial\emptyset}{\partial t} = M_\emptyset\left(\nabla\varepsilon^2\nabla\emptyset - p(\emptyset)\begin{bmatrix}(1-C_L)H^A\\ +C_L H^B\end{bmatrix} + [1-p(\emptyset)]\begin{bmatrix}(1-C_S)\\ +C_L H^B\end{bmatrix}\right) \quad (10)$$

$M_\emptyset$ is the phase field mobility, H^A is expressed as:

$$H^A = W^A g'(\emptyset) + 30g(\emptyset)L^A\left(\frac{1}{T}-\frac{1}{T_m^A}\right) \quad (11)$$

H^B has similar expressions to H^A.

Based on the WBM II model, the expression refines and calculates the solute concentration at the interface region, which changes the WBM II model's thought that the solid-liquid interface region is composed of the same solid and liquid mixture. When it is assumed that the solid and liquid solute concentration at the interface ($C_S = C_L$)is the same, it is the original WBM II model.

2.2 Solute diffusion equation

$$\frac{\partial C}{\partial t} = \nabla M_C\left[\frac{V_m}{R}\frac{\nabla C}{c(1-c)} + (H_B - H_A)\nabla\emptyset - \nabla(\delta^2\nabla^2 C)\right] \quad (12)$$

where M_C is the solute field mobility, the solute concentration C at the interface region is the sum of the solid and liquid phases concentration and their mass fractions. When the two phases are balanced, the chemical potentials of the solid and liquid phases at the any point of interface region are equal.

$$C = p(\emptyset)C_S + (1-p(\emptyset))C_L \quad (13)$$

$$\mu^S(C_S(x,t)) = \mu^L(C_L(x,t)) \quad (14)$$

2.3 Thermal diffusion equation

In this model, the calculation of the temperature field is coupled at the same time:

$$\frac{\partial T}{\partial t} = D_T\nabla^2 T - \frac{L^A(1-C)+CL^B}{C_p}p'(\emptyset)\frac{\partial\emptyset}{\partial t} - \frac{L^A-L^B}{C_P}(1-p(\emptyset))\frac{\partial C}{\partial t} \quad (15)$$

where D_T is the thermal diffusiviy, C_p is the specific heat.

3. Selection and determination of calculation parameters

3.1 Determination of phase field parameters

The functional relation between the calculation parameters M^A, M^B, W^A, W^B, $\bar{\varepsilon}$ can be obtained by defining the interface energy σ and the interface thickness ξ. By solving the phase field equations, the functional relation between the calculation parameters M^A, M^B, W^A, W^B, $\bar{\varepsilon}$ and the thermal physical parameters of the alloy can be expressed as:

$$M^A = \frac{(T_m^A)^2\beta^A}{6\sqrt{2}L^A\xi^A}M^B = \frac{(T_m^B)^2\beta^B}{6\sqrt{2}L^B\xi^B} \quad (16)$$

$$W^A = \frac{3\sigma^A}{\sqrt{2}T_m^A\xi^A}W^B = \frac{3\sigma^B}{\sqrt{2}T_m^B\xi^B} \quad (17)$$

$$\bar{\varepsilon}^2 = \frac{6\sqrt{2}\sigma^A\xi^A}{T_m^A} = \frac{6\sqrt{2}\sigma^B\xi^B}{T_m^B} \quad (18)$$

where σ^A, σ^B is the interface energy of component A and B, respectively; T_m^A, T_m^B is the melting point of component A and B, respectively; ξ^A, ξ^B is the interface thickness of component A and B, respectively; β^A, β^B is the linear interface dynamic coefficient of component A and B, respectively; M^A, M^B is the variable of component A and B related to the phase field mobility, respectively; $\bar{\varepsilon}$ is the mode number of phase field gradient energy coefficient.

3.2 Disturbance selection

In this paper, by adding thermal disturbance at the interface to simulate the various fluctuations of the interface region in the actual solidification process, it is closer to the physical process of the real alloy solidification. The method of introducing thermal disturbance is expressed as:

$$\frac{\partial C}{\partial t} \rightarrow \frac{\partial C}{\partial t} + 16g(\emptyset)\chi\alpha C \quad (19)$$

where χ is a random number whose value is uniformly distributed between -1 and +1; α is thermal disturbance amplitude, and the disturbance intensity can be adjusted according to the distance from the interface region, so that the disturbance only occurs at the solid-liquid interface. The thermal disturbance introduced by this method can clearly simulate the morphology evolution of the interface and the distribution law of the solute field.

3.3 Correction of interface thickness

In the phase-field model, the smaller interface thickness will significantly increase the simulation time, and the larger interface thickness will cause the simulation result to deviate from the real. Therefore, the selection of the interface thickness should meet the accuracy requirement as much as possible and take into account the calculation efficiency. Therefore, based on the definition of interface thickness ξ in the WBM II model, this paper modifies and refines the interface thickness. By introducing other regulatory variables, the interface thickness parameters have different sizes at different times and locations of dendrite growth, so this method can simulate dendrites in detail and accurately.

The modified interface thickness ξ is expressed as:

$$\xi d = \xi + \tau d \tag{20}$$

where d isthe thickness of solute diffusion layer at the interface front; τ is the influence coefficient of the diffusion layer thickness to the interface thickness.

4. Numerical calculations

4.1 Initial condition and boundary condition

The initial nucleus radius is r_0 the initial condition and the boundary condition can be expressed as:

$$x^2 + y^2 \le r_0^2 \emptyset = 0, \mu = 0, C = C_0; \tag{21}$$

$$x^2 + y^2 \ge r_0^2 \emptyset = -1, \mu = -\Delta, C = C_0; \tag{22}$$

where x, y is the horizontal coordinate and the vertical coordinate, respectively; Δ is the dimensionless undercooling; C_0 is the initial composition of alloy.

The Zero-Neumann boundary condition[20,21,22] is selected in the phase field calculation region boundary.

4.2 Numerical calculation method

In the simulation, the explicit finite difference method is used to solve the phase field equation and solute field equation, respectively and the thermal diffusion equation is solved by the alternating implicit scheme. Only one quarter of the dendrite growth region is calculated. The number of calculated grids of phase field and solute field is 800× 800, and the grid size is 4×10^{-7}m.

4.3 Physical parameters

The physical parameters of the Ni-Cu alloy used in the simulation are listed in Table 1.

Table 1 Physical parameter of Ni-Cu alloy.

Parameter/Unit	Value
T_m/K	1728
σ/(J/cm)	3.7×10^{-5}
β/(cm/ks)	0.33
D_T/(cm^2/s)	0.155
C_P/(J · K · cm^{-3})	5.0
V_m/(cm^3/mol)	7.4

5. Results and discussion

5.1 Influence of the interface thickness coefficient on the dendritic growth

In the modified interface thickness ξ , we use τ to indicate the influence coefficient of the diffusion layer thickness to the interface thickness. It reflects the degree of change in interface thickness resulting from changes in the diffusion layer thickness at interface frontier in all interface regions. In the simulation of dendrite growth, the interface thickness is a key influence factor in the theory of dendrite growth. But so far, the relationship between the setting of the interface thickness and the physical parameters cannot be accurately obtained by experimental methods. Therefore, this paper provides a theoretical basis for determining the relationship between interface thickness and physical parameters by studying the relationship between interface thickness and dendrite growth behavior.

Fig.1 shows the morphology of temperature field, dendritic growth and solute field under different influence coefficients when $\xi = 12\Delta_x$ and t = 45000Δt. It can be seen from Fig.1(a_2) that when the influence coefficient τ = 0.012, all growth directions of the interface are stable, the interface direction is continuous and the dendrites trunk are smooth. As the influence coefficient τ increases, the dendrite trunk becomes slender, the dendrite tip growth velocity increases, and the curvature radius decreases. At the same time, the secondary dendrites begin to appear and gradually become more and riper, as shown in Fig. 1(b_2). When the influence coefficient τ is increased to 0.018, the growth of the intersection of the main branches and its high-order dendrites is missing, the interface curve becomes discontinuous at the intersection and the dendrite tip appears edges with curvature radius decreases, as shown in Fig. 1(c_2).It can also be seen from Fig. 1 that with the increase of the influence coefficient τ , the number and the size of secondary dendrites increases due to the fact that the disturbance on the dendrite trunk makes the smooth interface appear dendritic sprout. The addition of the influence coefficient τ will reduce the interface thickness in this region, so that the high-order dendrite sprouts grow more easily. Therefore, the number of secondary dendrites increases accordingly.

In order to quantitatively analyze the influence of τ on dendrite growth morphology, we calculate the dendrite tip velocity, tip radius and solute concentration with influence coefficient τ , respectively.

Fig. 2 shows the curve of dendrite tip velocity, tip radius, solid fraction and segregation ratio under different influence coefficients. It can be seen from Fig. 2a, c, d that the dendrite tip velocity, solid fraction and segregation ratio increase with the increase of the influence coefficient, while the tip radius decreases with the increase of the influence coefficient, as shown in Fig. 2b. This is because as the influence coefficient τ increases, the interface thickness of dendrite tip gradually decreases and the interface thickness at the dendrite intersection gradually increases. This causes the growth rate of the dendrite tip to increase rapidly, while the growth rate is almost constant at the non-tip and intersection regions, thus reducing the curvature radius of the dendrite tip. When the influence coefficient τ increases to 0.018, the growth rate of the dendrite tip reaches the maximum, the solute precipitated during solidification is enriched at the solid-liquid interface frontier around the tip and the growth rate of the dendrite is greater than the diffusion rate of the solute, so the solute trapping effect is more and more obvious, which leads to the increase of the highest solute concentration and the solute concentration gradient at the dendrite tip interface frontier.

5.2 Effect of interface thickness on dendritic morphology and tip behavior

The interface thickness has an important influence on the temperature distribution at the interface, the morphology and gradient of the solute diffusion during dendrite growth. Therefore, based on the modification and analysis of interface thickness, we study the dendritic growth morphology and tip steady state behavior of Ni-Cu alloy under different interface thicknesses in this paper.

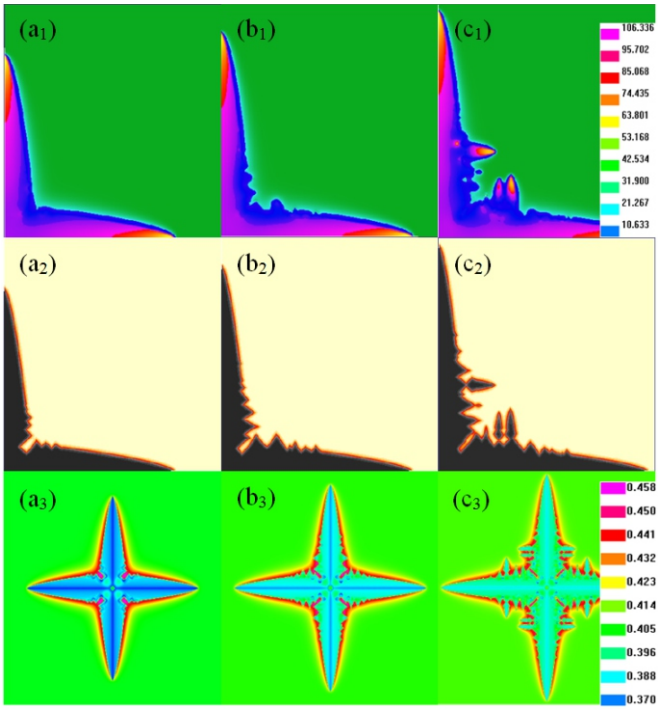

Fig. 1 Morphology of temperature field(a_1,b_1,c_1), dendritic growth (a_2,b_2,c_2) ,solute field (a_3, b_3, c_3) under different influence coefficients τ and (a_1, a_2, a_3) τ = 0.012; (b_1, b_2, b_3) τ = 0.015; (c_1, c_2, c_3) τ = 0.018, respectively.

Fig.3 shows the morphology of temperature field, the morphology of dendrite growth and the morphology of solute field distribution under different interface thicknesses. It can be seen from Fig. 3(c_2) that when the interface thickness $\xi = 12\Delta x$, the dendrite growth is most developed, and the dendrite not only has a developed secondary dendrite arm, but also has a fine primary dendrite trunk. With the interface thickness increases, the number of secondary dendrite arms decreases and becomes smaller, while the primary dendrite trunk is also thicker, as shown in Fig. 3(b_2). When the interface thickness increases to $18\Delta x$ a small amount of slightly raised secondary dendrites are seen only at the root of the primary dendrite, as shown in Fig. 3(a_2). This indicates that reducing the interface thickness promotes the growth of dendrites, meanwhile the secondary dendrite arms are more developed, and the growth of the secondary dendrite arms and the increase in the growth rate of the dendritic tips make the primary dendritic trunks finer.

It can be seen from Fig. 3(a_1) and (a_2) that the solute distribution is consistent with the phase field morphology. From the solute distribution point of view, the Cu concentration in the primary branch center is relatively low due to the undercooling caused by the dendrite tip curvature effect, which causes the solidus line to move downward. Enrichment of solute Cu occurs at the solid-liquid interface front of dendritic solidification. This is due to the redistribution of solute during the solidification process of the alloy, resulting in the concentration of Cu in the solid phase being lower than its initial concentration, while the extra Cu element can only enter the liquid phase in the front of the interface through the interface region. Since the solute diffusion rate in the liquid phase is much smaller than the dendrite growth rate, resulting

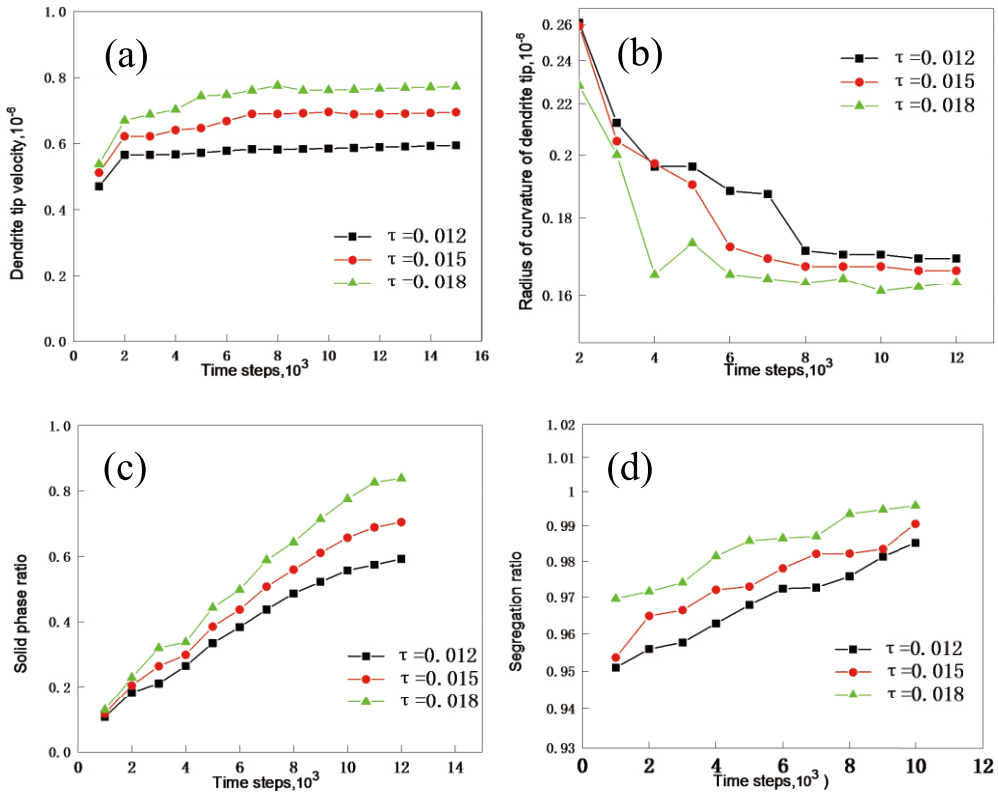

Fig. 2 The curve of (a) dendrite tip velocity, (b) tip radius, (c) solid fraction, and (d) segregation ratio under different influence coefficients.

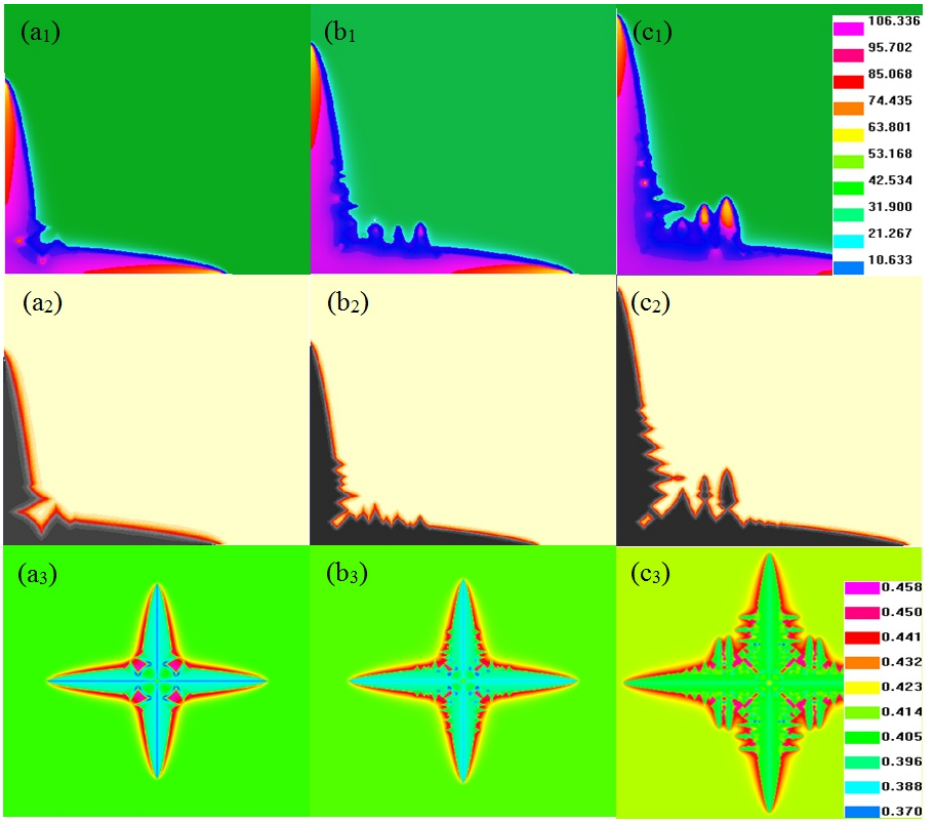

Fig.3 Morphology of temperature field (a_1, b_1, c_1), dendritic growth (a_2, b_2, c_2), solute field (a_3, b_3, c_3) under different interface thickness, among them (a_1, a_2, a_3) $\xi = 18\Delta x$; (b_1, b_2, b_3) $\xi = 15\Delta x$; (c_1, c2, c_3) $\xi = 12\Delta x$, respectively.

in the solute precipitated during solidification cannot be sufficiently diffused into the liquid phase and to be concentrated at the front edge of the dendrite interface. As the interface thickness increases, the excess Cu on the interface front will be more difficult to diffuse into the liquid phase region at the interface front through the interface region, resulting in a rapid increase of the highest solute concentration at the tip of the dendrite. At the same time, the decrease of the solute concentration gradient on the liquid phase side of the interface frontier caused by the increase of the interface thickness at the interface region will further increase the difficulty of solute diffusion. Therefore, from the perspective of solute diffusion, as the interface thickness increases, the growth rate of dendrites will gradually slow down. At the same time, a larger interface thickness will also increase the stability of the interface, so that the secondary dendrite sprouting caused by the random perturbation does not easily develop into a secondary dendrite. Thus, as the interface thickness increases, the growth rate of dendrites slows down, and the volume and number of secondary dendrites also decrease significantly.

6. Conclusions

(1) The definition of the solute concentration at the interface region was modified in the WBM II model. By setting the same chemical potential in the solid and liquid phases at the interface, but the solute concentration is different. The solute concentration at the interface region was further defined and analyzed. The modified model is more consistent with the actual solidification process, and can realistically simulate the growth law of dendrites. The introduction of disturbance enables it to simulate complex dendrite growth morphology such as secondary or higher-order arm growth.

(2) The interface thickness parameter was modified so that the interface thickness had different values in different parts of the dendrite growth. The modified model is more practical. By studying the influence of the interface thickness on the thickness of solute diffusion layer at the interface front, it reveals an important relationship between the morphology of the dendritic growth process and the solute diffusion at the interface frontier.

(3) The decrease of the interface thickness can promote the growth of dendrites and the emergence and growth of the secondary dendrite arms and the growth of the secondary dendrite arms make the dendrite trunk thinner. As the thickness of the interface increases, the highest solute concentration and solute gradient at the interface frontier are reduced. This makes it more difficult for the solute diffused from the solid to liquid at the interface frontier, resulting in retardation of dendrite growth.

(4) In the actual solidification process, the dendrite growth process is carried out in three dimensions and considering external fields (flow fields, magnetic fields, pressure fields, etc.). In order to accurately simulate the dendritic growth process, we still need to improve our model.

Acknowledgments

This work is supported by the National Natural Science Foundation of China (Nos.51774254, 51774253, 51701187, U1610123, 51674226, 51574207, and 51574206), The Science and Technology Major Project of Shanxi Province (No.MC2016-06). and supported by the fund of the State Key Laboratory of Solidification Processing in NWPU(SKLSP201802).

References

1. L. F. Du, Thesis phase field study of the metallic solidification in complex conditions, Northwestern Polytechnical University, Xi'an, China, 2014.
2. H. Yuan, Numerical simulation of dendritic growth of Ni-Cu binary single-phase alloys using a phase-field method, Harbin Institute of Technology, Harbin, China, 2010.
3. S. Y. Pan, M. F. Zhu, M. Rettenmayr, *Acta. Mater*., 2017, **13**, 2565-575
4. M. Asta, C. Beckermann, A. Karma, W. Kurz, R. Napolitano, M. Plapp, G. Purdy, M. Rappaz and R. Trivedi, *Acta. Mater.*, 2009, **57**, 941-971
5. A. A. Wheeler, W. J. Boettinger and G. B. Mcfadden, *Phys. Rev. A*, 1992, **45**, 7424-7439
6. A. A. Wheeler, W. J. Boettinger and G. B. Mcfadden, *Phys. Rev. E*, 1993, **47**, 1893-1909
7. W. J. Boettinger, A. A. Wheeler, B. T. Murray and G. B. Mcfadden, *Mater. Sci. Eng. A*, 1994, **178**, 217-223
8. J. A. Warren, W. J. Boettinger, *Phys. Rev. A*, 1991, **43**, 1310-1317
9. S. G. Kim, W.T. Kim and T. Suzuki, *Phys. Rev. E*, 1998, **58**, 3316-3323
10. A. Karma, W. J. Rappel, *Phys. Rev. Lett*., 1996, **77**, 4050-4053
11. B. Echebarria, A. Karma, R. Folch and M. Plapp, *Phys. Rev. E*, 2004, **70**, 061604
12. I. Loginova, G. Amberg and J. Agren, *Acta. Mater*., 2001, **49**, 573-581
13. N. Provatas, M. Greenwood, B. Athreya, N. Goldenfeld and J. Dantzig, *Int. J. Mod. Phys. B*., 2005, **19**, 4525-4565
14. X. H. Wu, G. Wang, L. Z. Zhao, D. C. Zeng and Z. W. Liu, *Comp. Mater. Sci*., 2016, **117**, 286-293
15. L. F. Du, P. Zhang, S. M. Yang, Z. T. Gao, J. Chen and H. L. Du, *Appl. Phys. A*., 2018, **124**, 211-216
16. C. J. Hou, Y. C. Jin, Y. H. Zhao, H. Hou and L. L. Tong, *Chin. J. Nonferrous. Met*., 2016, **26**, 60-65
17. Y. H. Zhao, W. J. Liu and H. Hou, *Rare. Metal. Mat. Eng*., 2014, 43, 841-845
18. H. Wang, Y.H. Zhao, B. Zhang, W. P. Chen and H. Hou, *Foundry. Techno.*, 2018, **39**, 760-768
19. J. A. Warren and W. J. Boettinger, *Acta. Metall*., 1995, **43**, 689-703
20. W. Kurz and D. J. Fisher, Fundamentals of Solidification, 4th Edn., *Higher Education Press*, Beijing, China, 2010.
21. Y. S. Kang, Y. H. Zhao, H. Hou, Y. C Jin and L. W. Chen, *PFM J. Acta Physica Sinica*, 2016, 65.
22. Y. H. Zhao, W. J. Liu and H. Hou, *J. Rare. Metal. Mat. Eng.*, 2014, **43**, 841-845